Article

Cell Reports

Infection Reveals a Modification of SIRT2 Critical for Chromatin Association

Graphical Abstract

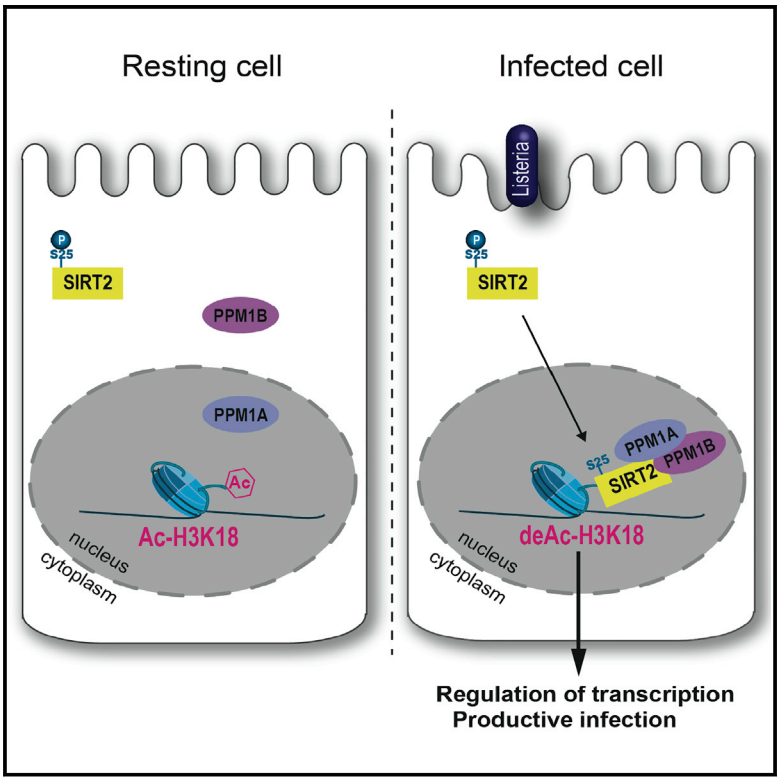

Authors

Jorge M. Pereira, Christine Chevalier, Thibault Chaze, ..., Mariette Matondo, Pascale Cossart, Mélanie A. Hamon

Correspondence

pascale.cossart@pasteur.fr (P.C.), melanie.hamon@pasteur.fr (M.A.H.)

In Brief

Sirtuins are enzymes critical for various processes, including genomic stability, metabolism, and aging. Through study of *Listeria monocytogenes,* a bacterial pathogen that exploits SIRT2 for productive infection, Pereira et al. uncover a SIRT2 modification necessary for chromatin association and function.

Highlights

- Infection induces modification of the host deacetylase SIRT2 to target it to chromatin
- Dephosphorylation of serine 25 on SIRT2 controls its subcellular localization
- PPM1A and PPM1B form a nuclear complex to dephosphorylate serine 25
- The phosphorylation state of serine 25 is crucial for *Listeria* infection

Pereira et al., 2018, Cell Reports *23*, 1124–1137
April 24, 2018
https://doi.org/10.1016/j.celrep.2018.03.116

CellPress

OPEN ACCESS
CellPress

Cell Reports
Article

Infection Reveals a Modification of SIRT2 Critical for Chromatin Association

Jorge M. Pereira,[1,2,3,4] Christine Chevalier,[4] Thibault Chaze,[5] Quentin Gianetto,[5] Francis Impens,[1,2,3,6] Mariette Matondo,[5] Pascale Cossart,[1,2,3,*] and Mélanie A. Hamon[4,7,*]

[1]Institut Pasteur, Unité des Interactions Bactéries-Cellules, Paris, France
[2]Institut National de la Santé et de la Recherche Médicale, U604, Paris, France
[3]Institut National de la Recherche Agronomique, USC2020, Paris, France
[4]Institut Pasteur, Chromatine et Infection G5, Paris, France
[5]Institut Pasteur, Unité de Spectrométrie de Masse Structurale et Protéomique, Paris, France
[6]Center for Medical Biotechnology, VIB, Ghent University, 9000 Ghent, Belgium
[7]Lead Contact
*Correspondence: pascale.cossart@pasteur.fr (P.C.), melanie.hamon@pasteur.fr (M.A.H.)
https://doi.org/10.1016/j.celrep.2018.03.116

SUMMARY

Sirtuin 2 is a nicotinamide-adenine-dinucleotide-dependent deacetylase that regulates cell processes such as carcinogenesis, cell cycle, DNA damage, and infection. Subcellular localization of SIRT2 is crucial for its function but is poorly understood. Infection with the bacterial pathogen *Listeria monocytogenes*, which relocalizes SIRT2 from the cytoplasm to the chromatin, provides an ideal stimulus for the molecular study of this process. In this report, we provide a map of SIRT2 post-translational modification sites and focus on serine 25 phosphorylation. We show that infection specifically induces dephosphorylation of S25, an event essential for SIRT2 chromatin association. Furthermore, we identify a nuclear complex formed by the phosphatases PPM1A and PPM1B, with SIRT2 essential for controlling H3K18 deacetylation and SIRT2-mediated gene repression during infection and necessary for a productive *Listeria* infection. This study reveals a molecular mechanism regulating SIRT2 function and localization, paving the way for understanding other SIRT2-regulated cellular processes.

INTRODUCTION

Originally identified in yeast as regulators of anti-aging genes, sirtuins form a family of highly conserved nicotinamide-adenine-dinucleotide (NAD)-dependent deacetylases. Seven mammalian sirtuins have been identified, and although they share a common catalytic domain, they are differentially localized in the cell. SIRT1—the closest homolog to yeast sirtuins—along with SIRT6 and SIRT7, is a nuclear protein, while SIRT3, SIRT4, and SIRT5 are exclusively found in mitochondria (Michan and Sinclair, 2007). SIRT2 was first shown to colocalize with microtubules in the cytoplasm but was also found in the nucleus under certain situations (North et al., 2003). The proper cellular localization of sirtuins is crucial for their function (Michan and Sinclair, 2007).

The function of SIRT2 has mainly been characterized in the cytoplasm, where it regulates microtubule dynamics, nuclear factor κB (NF-κB) signaling, and adipocyte differentiation by deacetylating, respectively, alpha-tubulin, p65, and the transcription factor FOXO1 (Gomes et al., 2015). Importantly, SIRT2 regulates cytoplasmic metabolism by sensing NAD levels and targeting proteins involved in metabolic homeostasis, such as aldolase and phosphoglycerate kinase (Cha et al., 2017; Gomes et al., 2015). Besides cytoplasmic substrates, SIRT2 has also been shown to target nuclear proteins, such as p53, the histone acetyltransferase p300, and various histones (Eskandarian et al., 2013; de Oliveira et al., 2012). SIRT2 has also been reported to be nuclear during mitosis, where it deacetylates histone H4 at lysine 16 to modulate chromatin condensation during the G2/M transition of the cell cycle while constitutively shuttling in and out of the nucleus in interphase cells (Inoue et al., 2007; North and Verdin, 2007a; Vaquero et al., 2006). However, the molecular features that dictate the substrate specificity of SIRT2 and its cellular localization remain completely unknown.

Entrance into the nucleus occurs through the nuclear pore complex (NPC), a macromolecular channel that limits free diffusion of proteins larger than approximately 40 kDa. Classically, larger proteins require binding to importin receptors that recognize primary amino acid sequences, called nuclear localization sequences (NLSs). The molecular mass of SIRT2, 43 kDa, which is close to the limit of size exclusion from the NPC, raises the question of whether SIRT2 is actively imported or diffuses freely into the nucleus. Sequence analysis has not revealed a canonical NLS motif for SIRT2, suggesting that nuclear import is not regulated (North and Verdin, 2007a). Nuclear localization can also be controlled by regulation of nuclear export, which is mediated by nuclear exporters such as the Chromosome region maintenance 1 (CRM1). SIRT2 has a nuclear export sequence (NES) and rapidly accumulates in the nucleus after treatment with Leptomycin B, a chemical inhibitor of the CRM1-dependent export (North and Verdin, 2007a), indicating that SIRT2 is actively exported from the nucleus. Removal of the NES from SIRT2 has a much greater effect on nuclear localization as compared to the addition of an NLS motif (Rothgiesser et al., 2010). NLS- and

NES-dependent transport can be regulated by mechanisms such as post-translational modifications (PTMs) of the cargo, including phosphorylation, methylation, and ubiquitination, but no such process has been described for SIRT2 (Martin et al., 2007; Terry et al., 2007; Xu and Massagué, 2004). Additionally, the lack of known stimuli inducing nuclear localization of SIRT2 has made the study of such a process difficult.

One recently identified stimulus, which led to the relocalization of SIRT2 to the nucleus, is infection with *Listeria monocytogenes* (Eskandarian et al., 2013). This bacterium is the causative agent of the disease listeriosis, which starts by the ingestion of contaminated food and is a problem mainly for immunocompromized patients and pregnant women. At the cellular level, *L. monocytogenes* is well adapted to exploit host cells for its benefit through very sophisticated mimicry and interactions with host proteins (Cossart, 2011). Our previous studies have shown that infection hijacks SIRT2, relocalizes it to the nucleus where SIRT2 associates to chromatin, and targets histone H3 for deacetylation on lysine 18 at the transcription start site of genes repressed during infection (Eskandarian et al., 2013; Figure 1A). Therefore, infection provides an optimal model to study the molecular mechanism of nuclear accumulation of SIRT2.

Previous reports have described phosphorylations of SIRT2, but these modifications did not alter its cellular localization (Nahhas et al., 2007; North and Verdin, 2007b). Therefore, we hypothesized that a yet-unidentified PTM of SIRT2 could be the molecular feature regulating nuclear localization. To address this point, we carried out a systematic identification of SIRT2 PTMs by mass spectrometry (MS), and we reveal Serine 25 phosphorylation as a critical modification site. The phosphorylation state of this residue determines SIRT2 chromatin association during *L. monocytogenes* infection. We identified the molecular complex assembled during infection, which dephosphorylates SIRT2-S25; it is composed of the phosphatases PPM1A and PPM1B. We further show that serine 25 dephosphorylation, and the activity of the underlying machinery is necessary for H3K18 deacetylation and transcriptional regulation during infection and essential for *L. monocytogenes* infection efficiency.

RESULTS

Amino Acids 1–37 Are Important for Chromatin Association of SIRT2 upon Infection

L. monocytogenes induces a relocalization of SIRT2 from the cytoplasm to chromatin, revealing a new role for SIRT2 in chromatin association and transcriptional regulation (Eskandarian et al., 2013; Figure 1A). SIRT2 is expressed as two major variants: the full-length protein, isoform 1 (398 amino acids [aa]), and a shorter splice variant, isoform 2 (352 aa), which lacks the first 37 aa (Figure 1B). To determine which isoform was being relocalized during infection, isoforms 1 and 2 were expressed separately as tagged proteins, and cellular localization was determined by immunoblotting cell fractionations of infected and control cells (Figures 1B and S1). While isoform 1 is present in the chromatin fraction in very small amounts in uninfected cells (less than 2%), 11% of the protein becomes relocalized to this fraction upon infection. In contrast, isoform 2 does not translocate to chromatin and is present at less than 2% in this fraction upon infection. Therefore, only isoform 1 associates with chromatin in infected cells, suggesting that a molecular feature contributing to nuclear localization is present in the first 37 aa and is absent from isoform 2.

We hypothesized that SIRT2 is post-translationally modified upon infection and used MS to identify such features. We immunoprecipitated SIRT2 (isoform 1) from cells that had been infected and fractionated, then we performed MS using higher energy collisional dissociation (HCD) fragmentation (Figure 1C). This analysis identified the 2 residues previously described as being modified, S368 and S372, but also several other modifications which had not been reported, including 12 serine and 2 threonine phosphorylation sites, 3 ubiquitinylation sites, and 6 acetylation sites. Of note, several of the phosphorylation sites were found on neighboring residues that are present on the same tryptic peptide. The low localization probability for these sites indicates that the exact location of the modified residue cannot be determined by HCD fragmentation of the peptide, leaving the possibility that only one of the neighboring residues is primarily modified (Figure 1C).

Interestingly for this study, a cluster of serine residues near the N terminus of SIRT2, present only in isoform 1, was detected as being phosphorylated in the cytoplasmic fraction but never in the chromatin fraction. Indeed, the presence of phosphopeptides, as depicted with a plus symbol in Figure 1C, was detected in the cytosol of infected cells, but only unmodified peptides, noted with a minus symbol in Figure 1C, were detected in the chromatin fraction. These results suggest that when SIRT2 isoform 1 is associated with chromatin upon infection, it is dephosphorylated on these residues.

SIRT2 Is Dephosphorylated on S25 upon Infection

Upon trypsin digestion, S23, -25, and -27 are present on the same peptide, and HCD fragmentation of this peptide cannot sort out which serine residue is phosphorylated. To determine which of these serine residues were modified, immunoprecipitated SIRT2 from whole-cell extracts was used for MS analysis using electron-transfer dissociation (ETD) as an alternative fragmentation method (Chi et al., 2007). Figure 2A shows a representative ETD spectrum of the tryptic SIRT2 phospho-peptide H_2N-$_{17}$VQEAQDS̲DS̲DS̲EGGAAGGEADMDFLR$_{42}$-COOH, clearly identifying S25 (indicated as an S below an asterisk) as the residue modified. Quantification of this phosphorylated peptide relative to the native peptide revealed that 45% of the detected SIRT2 peptide is phosphorylated at serine 25 in resting cells (Figure 2B). We further compared the phosphorylation levels between infected and uninfected cells and reveal a striking decrease in phosphorylated S25 but not phosphorylated S368 (Figure 2C). Therefore, we conclude that infection leads to a significant decrease in SIRT2 phosphorylation, specifically at S25.

S25 Dephosphorylation Is Necessary for Chromatin Association and H3K18 Deacetylation

In order to investigate the role of SIRT2 dephosphorylation in subcellular relocalization, we constructed a phospho-mimetic mutant of S25 (S25E), in which we also mutated adjacent S23

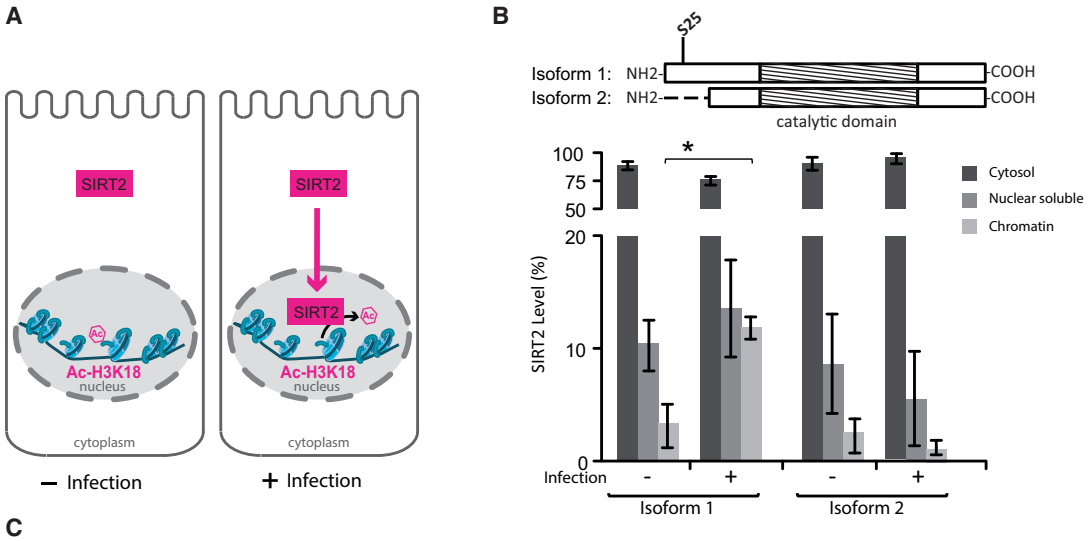

C

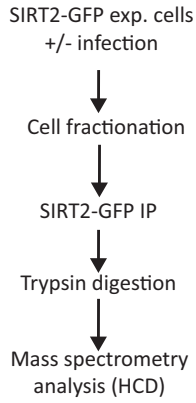

	Position	Location probability	Uninfected			Infected		
			Chromatin	Cytosol	Nucleus	Chromatin	Cytosol	Nucleus
Phospho	S23	0.33	-	-	-	-	+	-
	S25	0.33	-	-	-	-	+	-
	S27	0.33	-	-	-	-	+	-
	S50	0.47	+	+	-	-	+	+
	S53	0.98	+	+	-	-	+	+
	T63	1.00	+	-	-	-	-	-
	S88	0.69	-	-	-	-	+	-
	S100	0.96	-	+	+	-	+	-
	S226	1.00	-	-	-	-	+	-
	S351	0.66	+	+	+	-	+	+
	S356	0.99	+	+	+	+	+	+
	S364	0.62	+	+	+	+	+	+
	T365	0.57	+	+	+	+	+	+
	S366	0.85	+	+	+	+	+	+
	S368	0.99	+	+	+	+	+	+
	S372	1.00	+	+	+	+	+	+
Ub	K55	1.00	-	+	-	-	+	-
	K229	1.00	-	+	-	-	-	-
	K370	1.00	-	-	-	-	+	-
Acetyl	K55	1.00	-	+	-	+	+	+
	K126	1.00	-	+	+	+	+	+
	K158	0.98	-	+	-	-	+	+
	K210	1.00	-	+	-	-	+	-
	K229	1.00	-	+	-	-	-	+
	K371	1.00	-	+	-	-	+	+

Figure 1. SIRT2 Is Post-translationally Modified, and Chromatin Association Requires Amino Acids 1–37

(A) Schematic representation of the effect of *L. monocytogenes* on the subcellular localization of SIRT2. SIRT2 is mainly localized in the cytoplasm in uninfected conditions and translocates to the nucleus, where it associates with chromatin to cause H3K18 deacetylation at the transcriptional start site (TSS) of genes repressed during infection.

(B) Schematic representation of SIRT2 isoform 1 and isoform 2 and the identified serine 25 phosphorylation site. Isoform 1 is the full protein (389 aa), while isoform 2 lacks 37 aa from the N terminus. Histograms represent the mean SIRT2 levels in fractionated cells, immunoblotted and quantified in each fraction normalized to total SIRT2. Error bars represent SEM of at least 3 independent experiments. *$p < 0.05$, as measured with Student's t test. Both isoforms are present in the cytoplasm, but only isoform 1 associates to chromatin during infection.

(C) Flow diagram of the mass spectrometry experiment and a table listing SIRT2 modification sites identified in different subcellular fractions. Columns from left to right indicate the position of the modified serine (S), threonine (T), or lysine (K) residue in the SIRT2 protein sequence, the localization probability as a measure of the mapping precision of the identified modification, and an indication of whether the modification was detected (+) or not detected (–) in each of the subcellular fractions.

and S27 to glutamic acid in addition to serine 25 in order to minimize the compensatory effects of these residues. We also created a dephospho-mimetic mutant by changing the serine to a charged amino acid, alanine (S25A). Additionally, we generated a phospho-mimetic mutant of S368 (S368E) to use as a control in our assay. By fluorescence microscopy, we evaluated the cellular localization of these constructs with and without infection (Figure 3A). We observed that the S25E and S25A mutants were localized in the cytoplasm of uninfected cells as well as the wild-type (WT) SIRT2 and the S368E mutant. Upon infection, all the constructs could be detected in the nucleus, indicating that neither S25E nor S25A, nor S368E mutants are impaired in nuclear relocalization upon infection. Subcellular localization was then evaluated by cell fractionation, which separates the soluble nuclear fraction from the insoluble chromatin fraction, followed by western blotting (Figures 3B and S2). WT SIRT2

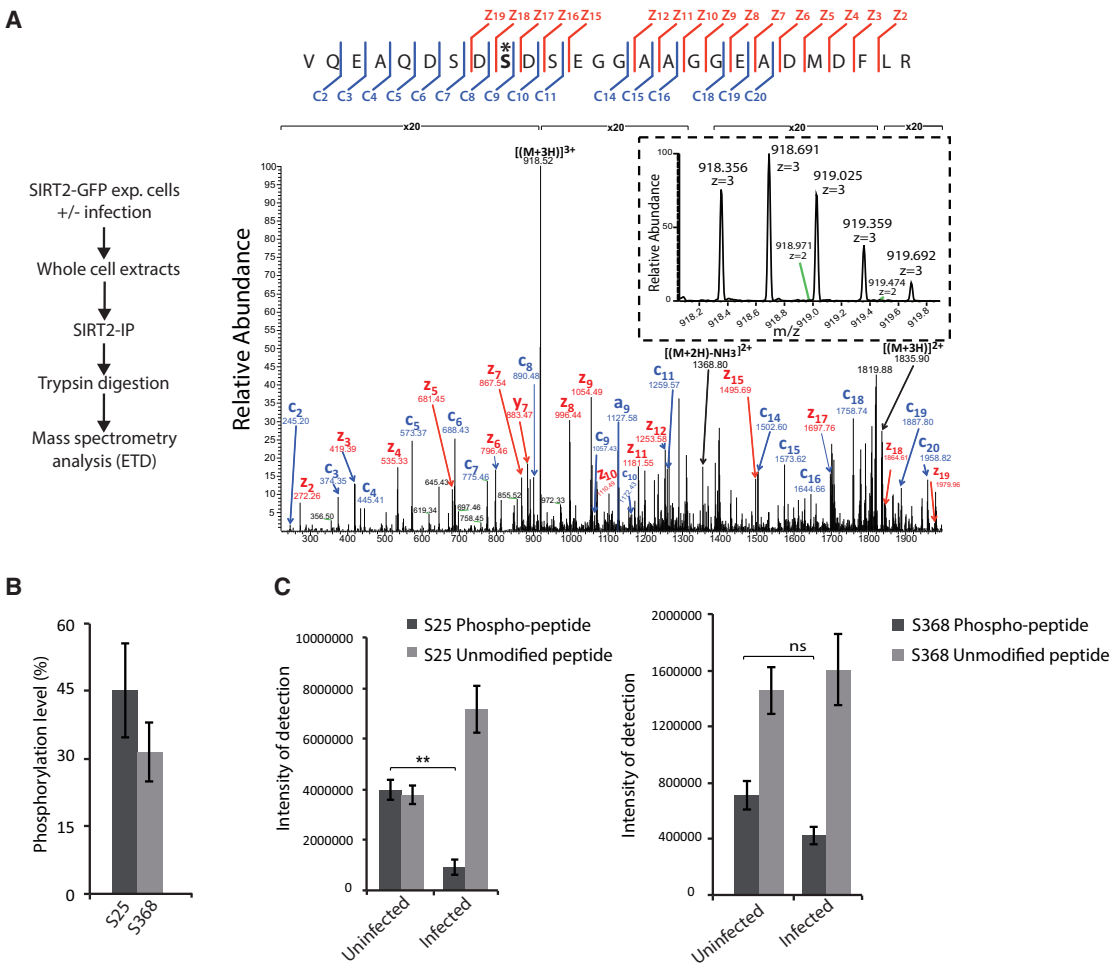

Figure 2. Serine 25 Is Dephosphorylated upon *Listeria* Infection

(A) Flow diagram of the mass spectrometry experiment and annotated ETD fragmentation spectrum of the identified tryptic SIRT2 peptide carrying the modified serine residue at position 25. The sequence of the peptide is shown above the spectrum, and matching c- and z-fragment ion series are indicated, clearly pointing toward S25 as the modified residue (highlighted by asterisk).

(B) Phosphorylation levels of the indicated peptide were calculated as the MS1 intensity of detection of phosphorylated peptide over that of both the modified and non-modified peptides. Error bars represent SEM of 3 technical replicates of at least 3 independent experiments.

(C) Intensity of detection of the peptide containing phosphorylated S25, phosphorylated S368, and the corresponding unmodified peptides as determined by ETD fragmentation. Error bars show SEM of 3 technical replicates of a representative experiment ($n \geq 3$). **$p < 0.01$; ns, $p \geq 0.05$, as measured with Student's t test.

and the S368E mutant strongly relocalize to the chromatin fraction upon infection. Strikingly the S25A mutant was also detected in the chromatin fraction upon infection, while a S25E mutant was not. Together, these data indicate that a mutant of SIRT2 that is locked in a pseudo-unphosphorylated state at S25 is able to associate to chromatin upon infection with *L. monocytogenes,* whereas a mutant locked in a pseudo-phosphorylated state is impaired.

SIRT2 activity is required for inducing H3K18 deacetylation and necessary for a productive *L. monocytogenes* infection (Eskandarian et al., 2013). In order to study the role of SIRT2-S25E in a background lacking endogenous SIRT2, we needed a cell line depleted of endogenous SIRT2 in which we could express SIRT2-S25E. To achieve this goal, we first generated SIRT2$^{-/-}$ and WT mouse embryonic fibroblasts (MEFs) and immortalized them by transformation with the simian virus 40 (SV40) large T antigen. These cell lines were assayed for their phenotype upon infection by quantifying the number of intracellular GFP bacteria per cell by fluorescence-activated cell sorting (FACS) analysis at 5 hr and 24 hr post-infection (Figure 3C). We observed that there was no significant difference between the levels of intracellular bacteria in WT and SIRT2$^{-/-}$ MEFs at 5 hr post-infection, suggesting no defect in invasion. However, at 24 hr post-infection, SIRT2 knockout MEFs showed 40% less intracellular bacteria compared to WT MEFs. These results are in agreement with our previous findings in infected epithelial cells inhibited for SIRT2 activity and our *in vivo* findings using SIRT2 knockout (KO) mice (Eskandarian et al.,

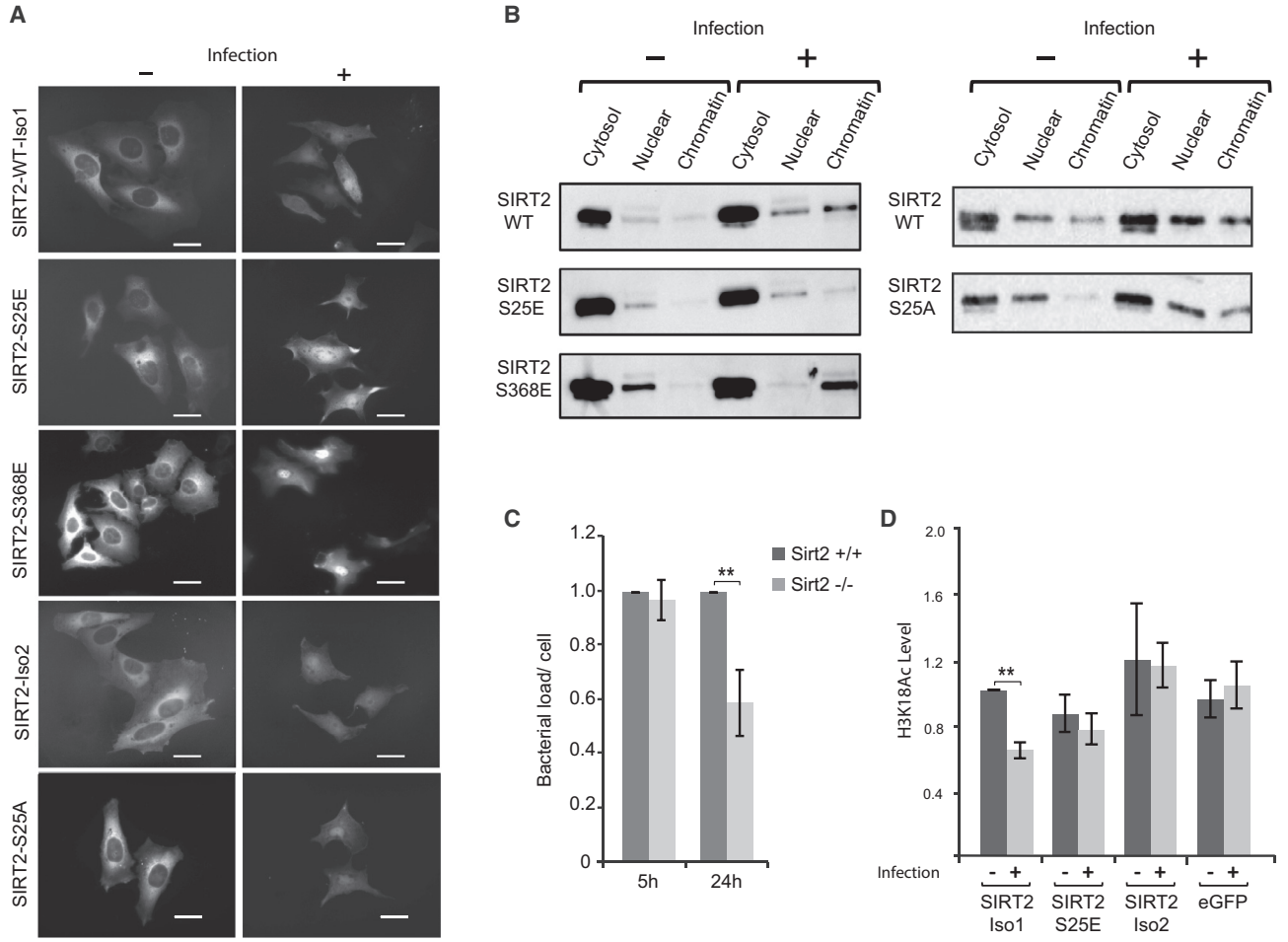

Figure 3. Serine25 Dephosphorylation Is Important for SIRT2 Relocalization and Activity at Chromatin

(A) Images of HeLa cells transfected with GFP fused to WT-SIRT2, SIRT2-S25E, SIRT2-S25A, SIRT2-S368E, and isoform 2, under uninfected (-) and infected (+) conditions. Scale bars, 10 μm.

(B) Cell fractionations of indicated SIRT2 mutants under uninfected (–) and infected (+) conditions. Representative image of n ≥ 3.

(C) WT MEFs or Sirt2$^{-/-}$ MEFs were infected with *L. monocytogenes* expressing GFP for the indicated times. Intracellular bacteria were detected by FACS analysis, and the geometric mean (mean fluorescence of intensity; MFI) of 10,000 cells was calculated. Results are normalized to uninfected cells and averaged over at least 3 independent experiments.

(D) Sirt2$^{-/-}$ MEFs were transfected with the indicated SIRT2 constructs, uninfected (dark gray), or infected (light gray) with *L. monocytogenes* for 5 hr. H3K18 acetylation levels were determined by immunoblotting and normalized to the total α-tubulin level.

Error bars represent SEM of at least 3 independent experiments. Statistical significance was calculated using a Student's t test. **p < 0.01.

2013). In order to assess the role of SIRT2 phosphorylation on H3K18 deacetylation during infection, we transfected SIRT2$^{-/-}$ MEFs with isoform 2, WT isoform 1, the S25E mutant, or an empty overexpression vector and quantified the H3K18Ac levels (Figures 3D and S3). We observed that, in cells complemented with WT isoform 1, H3K18Ac levels were lower after infection, indicating that this construct is able to induce H3K18 deacetylation *in vivo*. The small level of deacetylation observed reflects the low transfection efficiency in MEF cells (40%–50%). However, no decrease was observed with SIRT2-S25E or isoform 2, or by overexpression of EGFP tag alone. These results show that both the S25E mutant and isoform 2, which do not associate with chromatin, are impaired in H3K18 deacetylation during infection.

SIRT2 Interacts with PPM1A and PPM1B Phosphatases upon Infection

Phosphatases targeting SIRT2 have not been identified. In order to find the molecular players involved in SIRT2 dephosphorylation during infection, we immunoprecipitated SIRT2 and performed MS analysis on all proteins recovered. Our preliminary analysis suggested that SIRT2 interacts with PP2C phosphatases PPM1A and PPM1B (data not shown). To confirm the interaction of SIRT2 with these phosphatases, we performed co-immunoprecipitations from whole-cell lysates of cells overexpressing both SIRT2-GFP and PPM1A-FLAG. By immunoprecipitating SIRT2-GFP, PPM1A-FLAG was recovered, supporting the finding that the two proteins interact (Figure 4A). Interestingly, under these conditions,

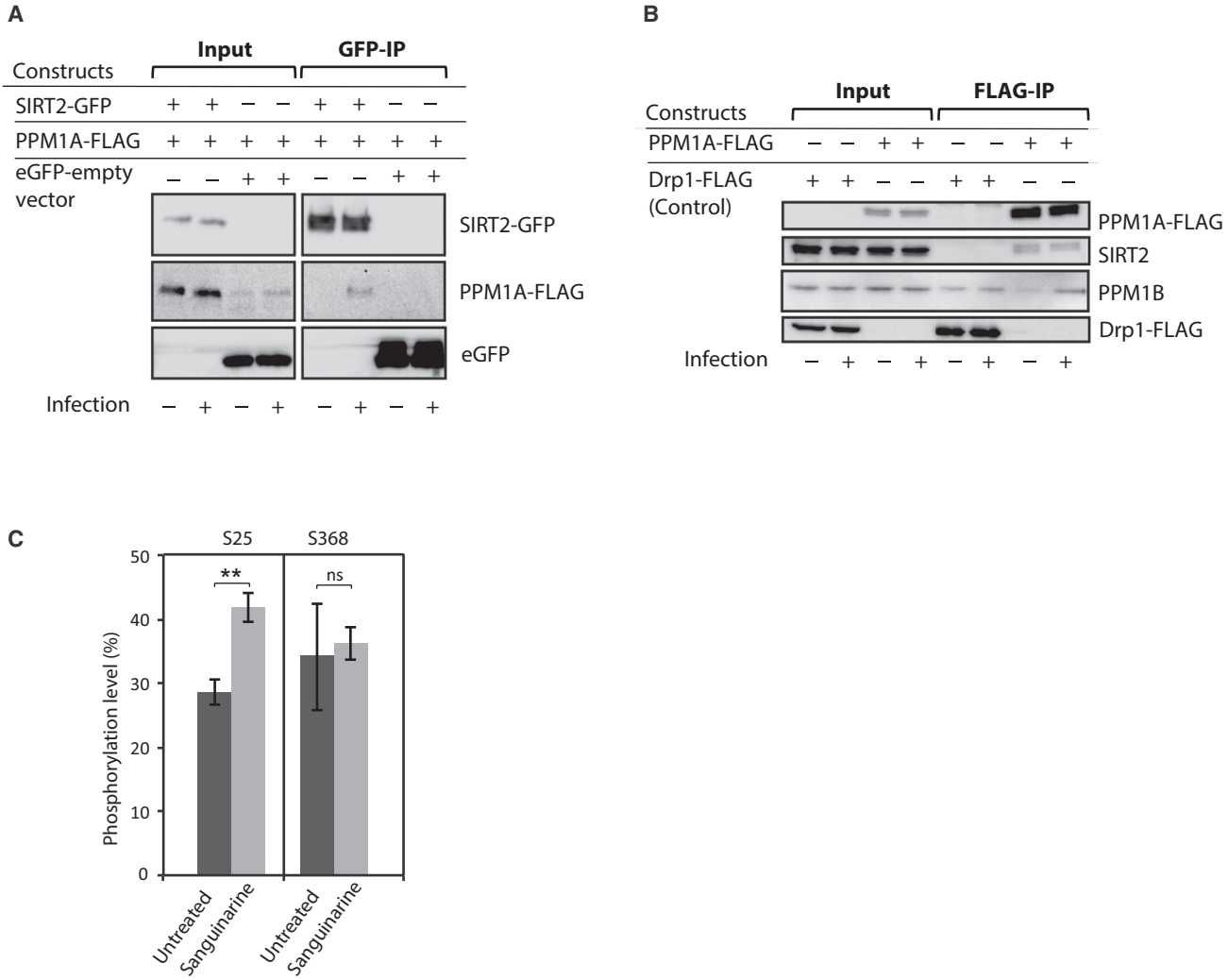

Figure 4. SIRT2 Interacts with Protein Phosphatases 1A and 1B upon Infection

(A and B) Shown here: (A) SIRT2-GFP and (B) PPM1A-FLAG immunoprecipitations under uninfected (–) and infected (+) conditions. Constructs are listed at the top, and antibodies are indicated next to the corresponding immunoblots. Images are representative of 3 experiments.

(C) Cells were treated with sanguinarine chloride for 24 hr. SIRT2 was immunoprecipitated and analyzed by mass spectrometry using ETD fragmentation. Phosphorylation levels of the indicated residue were calculated as the intensity of detection of phosphorylated peptide over that of both the modified and non-modified peptides.

Error bars represent SEM of 3 technical replicates of at least 3 independent experiments. Statistical significance was calculated using Student's t test. $^{**}p < 0.01$; ns, $p \geq 0.05$.

PPM1A is recovered mainly upon infection, suggesting that *L. monocytogenes* might enhance the interaction of PPM1A with SIRT2. We further performed co-immunoprecipitations to determine whether we could recover endogenous proteins (Figures 4B and S4). Upon overexpressing PPM1A-FLAG, both endogenous SIRT2 and PPM1B were recovered, and, upon overexpressing of a catalytically inactive PPM1B mutant (PPM1B-R179G-FLAG), a catalytically inactive PPM1B mutant was used to capture transient interactions (Chen et al., 2015; Kusuda et al., 1998), endogenous PPM1A was recovered. We used another protein, Drp1-FLAG, as a negative control in our immunoprecipitations and showed that, besides a slight interaction with PPM1B, no other proteins are recovered. Altogether, these results strongly support that PPM1A and PPM1B form a complex with SIRT2.

To determine the role of PPM1A and PPM1B in dephosphorylation of SIRT2, we treated cells with sanguinarine chloride, a pharmacological inhibitor of the PP2C phosphatase family (Aburai et al., 2010; Schaaf et al., 2017) and analyzed the levels of S25 and S368 phosphorylation by MS. By measuring the MS intensities of the phospho-peptides and normalizing to the total peptide intensity, we observed that the basal level of S25 phosphorylation increased significantly after sanguinarine treatment, whereas no significant change is observed for S368 (Figure 4C). These results indicated that the activity of PPM1A and PPM1B plays a role in the phosphorylation status of SIRT2 at S25.

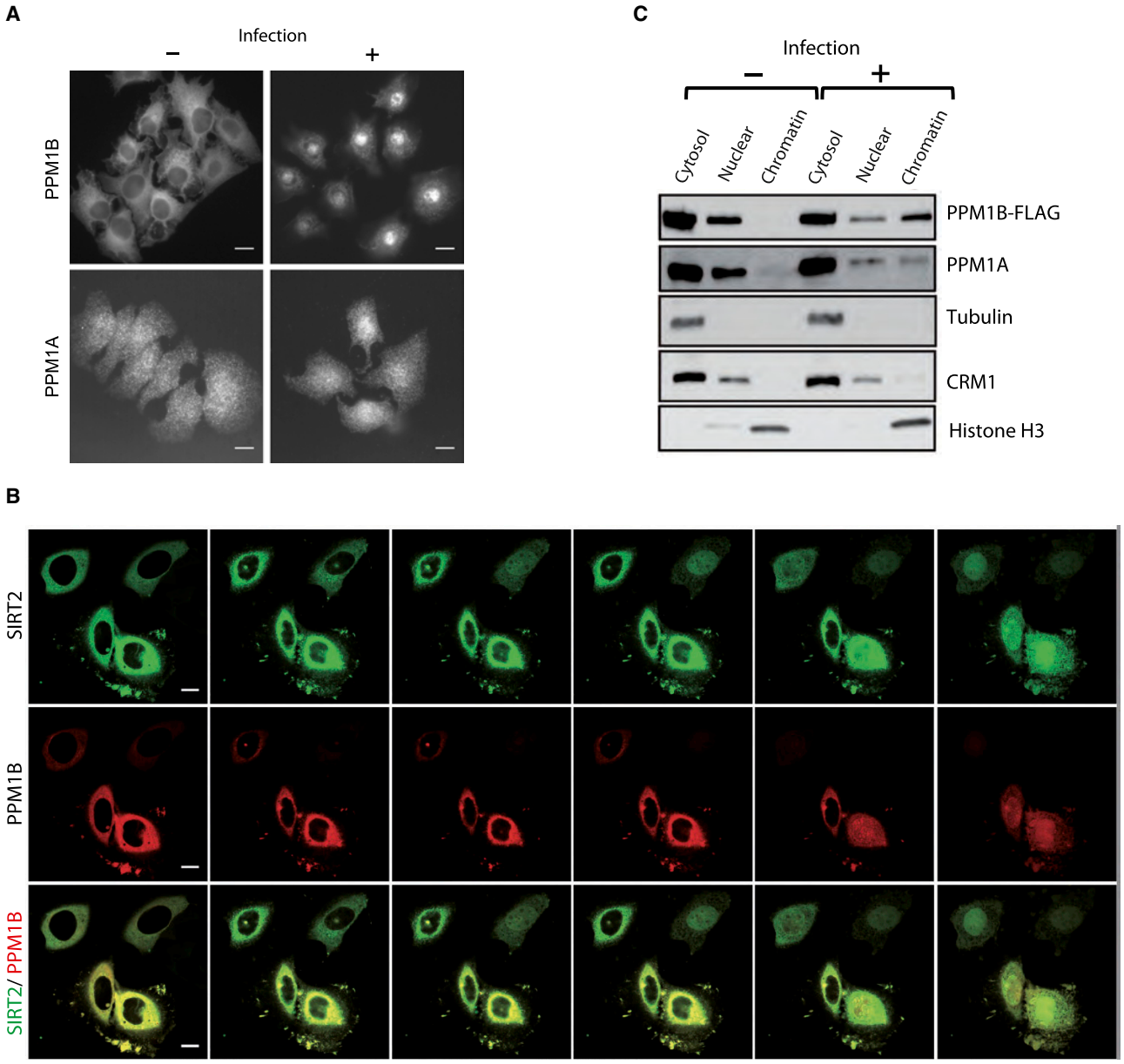

Figure 5. Protein Phosphatases 1A and 1B Relocalize to Chromatin upon Infection

(A) Immunofluorescence of endogenous PPM1B and PPM1A under uninfected (–) and 5-hr-infected (+) conditions. Scale bars, 10 μm.

(B) Live-cell imaging of HeLa cells showing SIRT2 (green) and PPM1B (red). Still images were acquired every 2 min after 1 hr of infection. Merged and single channels show the dynamics of SIRT2 and PPM1B subcellular localization during infection. Scale bars, 10 μm.

(C) Immunoblot of cell fractionation under uninfected (–) and 5-hr-infected (+) conditions. PPM1B-FLAG and endogenous PPM1A were revealed with antibodies against FLAG and PPM1A, respectively. Tubulin, CRM1, and histone H3 were used to control fraction purity. Image is representative of at least 3 experiments.

As SIRT2 relocalizes to the nucleus upon infection, we studied the cellular location of endogenous PPM1A and PPM1B (Figure 5A). Although PPM1A is detected both in the cytoplasm and the nucleus of uninfected cells, PPM1B is mainly detected in the cytoplasm. Upon infection, PPM1A staining does not significantly change. In contrast, PPM1B staining clearly becomes nuclear, suggesting that infection induces the relocalization of PPM1B protein to the nucleus (Figure 5A). We further focused on PPM1B for the study of the dynamics of relocalization upon infection. Live-cell imaging experiments were conducted in cells overexpressing WT SIRT2 and PPM1B before and after infection with *L. monocytogenes*. In uninfected cells, both SIRT2 and PPM1B remained localized in the cytoplasm of transfected cells (Figure S5). In infected cells, PPM1B and SIRT2 localized exclusively in the cytoplasm until 70 min post-infection (Figure 5B). Then, relocalization of both PPM1B and

SIRT2 occurred. By 82 min post-infection, all four imaged cells showed relocalization of both PPM1B and SIRT2 to the nucleus. This relocalization occurred in synchrony for PPM1B and SIRT2. The subcellular localization of the phosphatases was further characterized by fractionation of cells overexpressing WT PPM1B uninfected or infected with *L. monocytogenes* (Figure 5C). While both endogenous PPM1A and overexpressed PPM1B were absent from the chromatin fraction in uninfected cells, a strong band corresponding to these proteins was detected in this fraction in infected cells, indicating that, as for SIRT2, *Listeria* infection induces the relocalization of PPM1A and PPM1B to chromatin.

PPM1A and PPM1B Are Necessary for SIRT2 Dephosphorylation and Chromatin Association during Infection

We studied the role of PPM1A and PPM1B on SIRT2 phosphorylation during infection by blocking the activity of these phosphatases with sanguinarine and evaluating the levels of phosphorylated S25 and S368 by MS (Figure 6A). While infection decreased S25 phosphorylation levels from 25% to less than 5% in untreated cells, in cells treated with sanguinarine, infection only decreased phosphorylation levels from 40% to 30%, indicating that PPM1A and PPM1B inhibition blocked S25 dephosphorylation. This effect is specific to S25, as neither sanguinarine nor infection modified the levels of S368 phosphorylation.

Since serine 25 dephosphorylation is necessary for chromatin association, we studied the role of PPM1A and PPM1B in SIRT2 translocation to chromatin during infection. By fluorescence microscopy, SIRT2-GFP was monitored upon infection in the presence of sanguinarine (Figure 6B). Both in untreated and in sanguinarine-treated cells, we could observe that SIRT2 was localized in the cytoplasm in uninfected cells and relocalized to the nucleus upon infection to the same extent in both conditions. Cell fractionation was performed to measure the level of chromatin association of SIRT2 upon sanguinarine treatment (Figure 6C). Immunoblot analysis of the cellular fractions showed that sanguinarine treatment impairs chromatin association during infection, as compared to untreated cells. Therefore, blocking PPM1A and PPM1B activity with sanguinarine affected chromatin association but not translocation to the nucleus. These results are in agreement with our data showing that a phospho-mimetic S25E SIRT2 mutant is similarly impaired in translocation to chromatin.

PPM1B and PPM1A Are Necessary for SIRT2 Function during Infection

We next assessed the impact of PPM1A and PPM1B on SIRT2 function during infection. PPM1A and PPM1B were depleted by small interfering RNA (siRNA) treatment, or their activity was blocked with sanguinarine, and we evaluated the effect on infection-induced H3K18 deacetylation. In control siRNA, we observed a significant decrease in the levels of H3K18Ac upon infection, which did not occur in PPM1A and PPM1B siRNA-treated cells (Figure 7A). However, treating cells with siRNA against an unrelated phosphatase (PP1) had no effect on H3K18 deacetylation. In agreement with these results, cells treated with sanguinarine are also blocked in H3K18 deacetylation (Figure 7A).

The impact of PPM1A and PPM1B on *Listeria* infection was measured by quantifying bacterial levels upon siRNA or sanguinarine treatment. Cells were assayed 24 hr post-infection for the levels of a listerial housekeeping protein, EF-Tu, used as a readout of infection. Knocking down PPM1A or PPM1B with siRNA reduced intracellular *Listeria* levels by 40%, compared to control cells (Figure 7B), i.e., to the same extent as in knockout MEFs in Figure 4A. In agreement with these results, blocking PPM1A and PPM1B activities by sanguinarine treatment caused a similar reduction in *Listeria* levels.

Our previous studies by chromatin immunoprecipitation revealed that SIRT2 associated with the transcriptional start site of genes repressed during infection and that SIRT2 activity was necessary for gene repression upon infection (Eskandarian et al., 2013). To evaluate whether phosphorylation of S25 is necessary for transcriptional regulation by SIRT2, we characterized the role of PPM1A and PPM1B in this process after RNAi knockdown (Figure 7C). qPCR was used to evaluate the expression levels of genes previously shown to be regulated in a SIRT2-dependent manner. We compared PPM1B siRNA-treated cells to control cells upon infection. As we previously reported, we observed, in control cells, a significant expression level decrease for genes repressed during infection in a SIRT2-dependent manner (MYLIP, EHHADH, and ERCC5) and an increase for genes activated independently of SIRT2 (EMP1, TIPARP, and SDC4). Upon inactivation of PPM1B by siRNA knockdown, infection-induced repression was completely blocked. In contrast, infection-induced activation was not affected by siRNA treatment. Therefore, these results show that blocking PPM1B has a specific effect on genes repressed in a SIRT2-dependent manner.

DISCUSSION

In this study, we have performed a comprehensive analysis of SIRT2 PTMs and focused on serine 25 phosphorylation, which is located in the N-terminal part of SIRT2. Most notably, we revealed that dephosphorylation of S25 is necessary for SIRT2 chromatin association upon infection with the bacterium *L. monocytogenes*. We further identify two phosphatases, PPM1A and PPM1B, which dephosphorylate S25, form a complex with SIRT2 upon infection, and relocalize to the chromatin fraction simultaneously with SIRT2. Indeed, knocking out or inactivating the phosphatases phenocopies a SIRT2 knockout with regard to its effect on histone modifications, transcriptional regulation, and infection efficiency. S25 dephosphorylation is, therefore, essential for SIRT2 activity at the chromatin fraction during infection with *L. monocytogenes*.

Before our study, only two SIRT2 PTMs had been examined, S368 and S372 phosphorylation, and a few others had been identified by high-throughput phosphoproteomic screens (Flick and Lüscher, 2012; Hornbeck et al., 2015). S368, which is phosphorylated by the Cdk1 kinase, was shown to play a role in SIRT2-mediated mitotic delay, while no role has been identified for S372 phosphorylation (Nahhas et al., 2007; North and Verdin, 2007b). We had previously revealed new properties for SIRT2 in

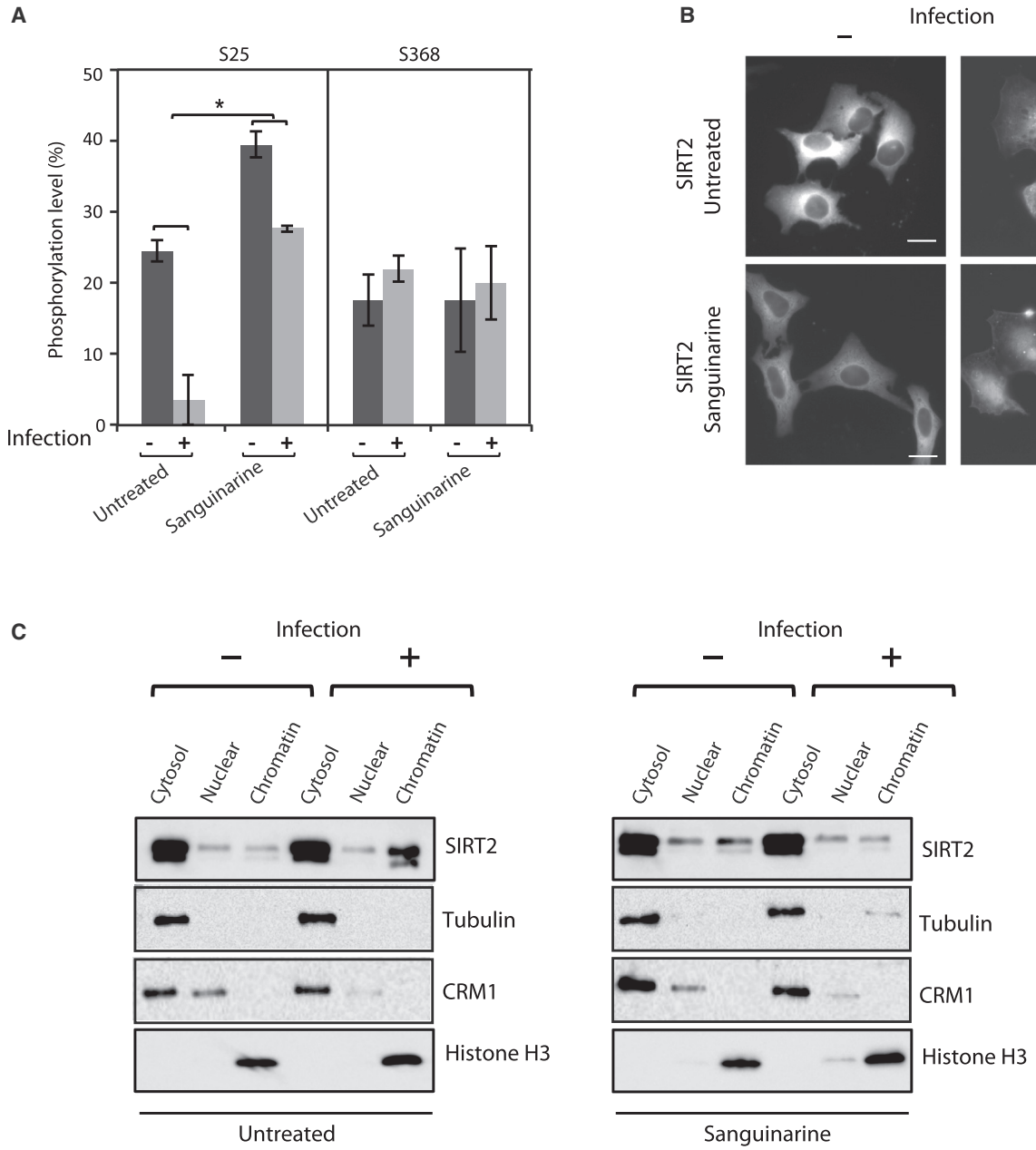

Figure 6. The Activity of PPM1A and PPM1B Is Necessary for SIRT2 Dephosphorylation and Chromatin Association

(A) SIRT2 was immunoprecipitated upon sanguinarine treatment from uninfected (−) or 5-hr-infected (+) cells and analyzed by mass spectrometry using ETD fragmentation. Phosphorylation levels of the indicated residue were calculated as the intensity of detection of phosphorylated peptide over that of both the modified and non-modified peptides.

(B) SIRT2-GFP images under uninfected (−) and 5-hr-infected (+). Scale bars, 10 μm. Experiments are representative of $n \geq 3$.

(C) Immunoblot of cell fractionation under uninfected (−) and 5-hr-infected (+) conditions. Tubulin, CRM1, and histone H3 were used to control fraction purity. Error bars represent SEM of at least 3 independent replicates. *$p < 0.05$, as measured with a Welch two-sample t test.

chromatin association, H3K18 deacetylation, and transcriptional regulation. We now show that S25 is the crucial residue that needs to be dephosphorylated to allow such SIRT2 activity and dictates SIRT2 subcellular localization.

In the literature, SIRT2 has been mainly characterized as a cytoplasmic deacetylase (North et al., 2003). Nuclear localization of SIRT2 has been observed in a very small percentage of resting cells and shown to accumulate in the nucleus upon Leptomycin B treatment (North and Verdin, 2007a). In fact, SIRT2 was shown to shuttle in and out of the nucleus in resting cells and be actively exported by Crm1-dependent nuclear export signal located in the N terminus between residues 41 and 51. We have previously

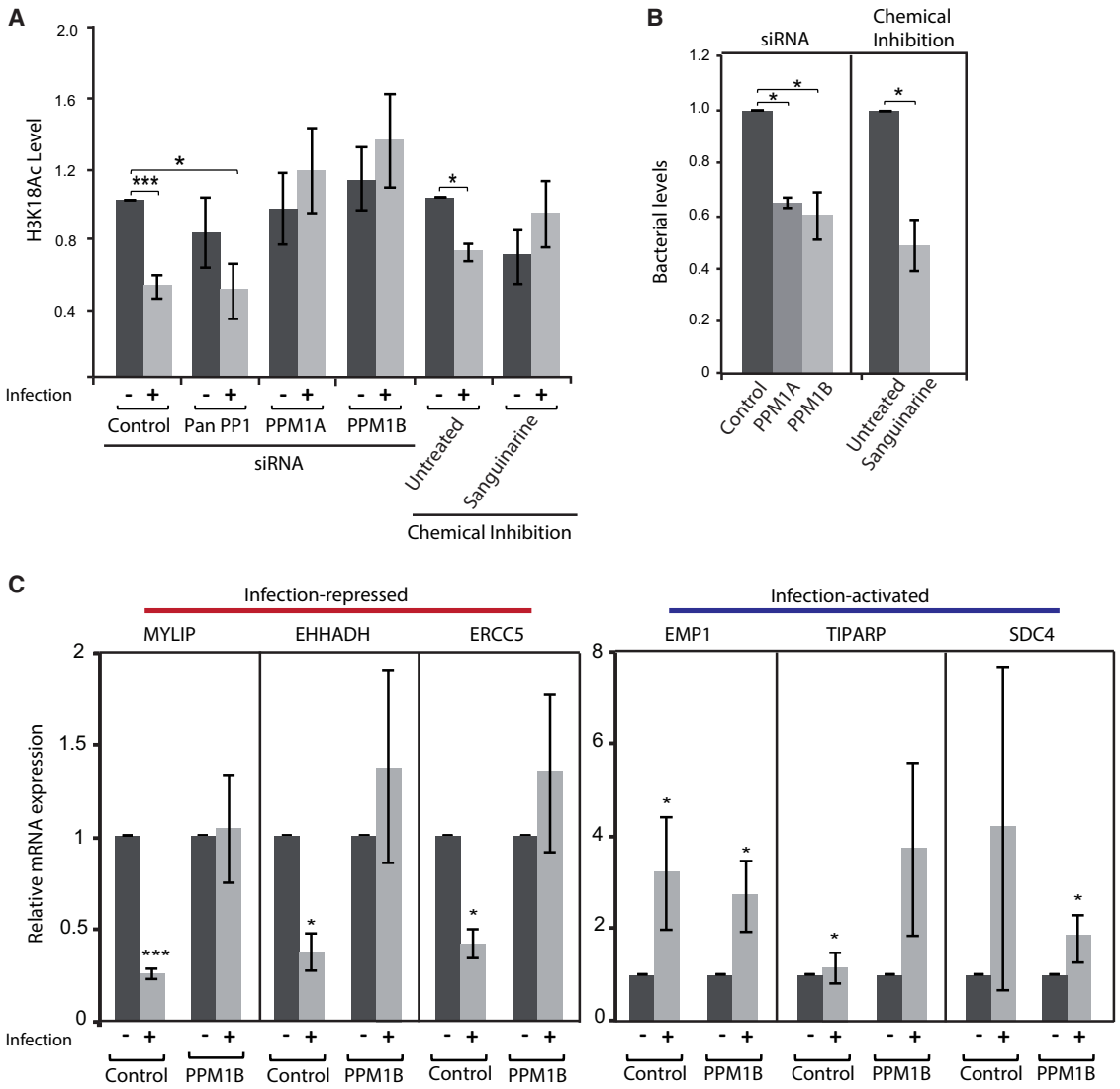

Figure 7. PPM1A and PPM1B Are Necessary for SIRT2 Function

(A) Immunoblots of cells transfected with the indicated siRNAs or preteated with sanguinarine chloride, uninfected (–) or 5-hr-infected (+).

(B) Bacterial levels as measured by immunoblotting against the Listerial protein EF-Tu in cells transfected with siRNA or treated with sanguinarine chloride. Cells were infected with *L. monocytogenes* EGD-e PrfA* for 24 hr. Quantifications of immunoblots are normalized to α-tubulin and to the control sample.

(C) Relative mRNA expression as detected by qPCR normalized to uninfected samples and to GAPDH. Infection-dependent repressed genes are highlighted in red, while infection-activated genes are highlighted in blue.

*$p < 0.05$; ***$p < 0.001$, as measured with Student's t test on the ΔCT values. Error bars represent SEM of at least 3 independent experiments.

shown that nuclear accumulation of SIRT2 with Leptomycin B does not lead to H3K18 deacetylation, suggesting that an additional signal is required for chromatin association (Eskandarian et al., 2013). The mechanism for nuclear accumulation, which is a prerequisite for chromatin association but is independent, is unknown but could involve one of the modifications that we identified by MS. It is notable from our data in Figure 3B that introducing a S368E mutation leads to higher nuclear localization of SIRT2 in resting cells; therefore, S368 phosphorylation could regulate this process. Interestingly, activation of Akt and phosphatidylinositol 3-kinase (PI3K), which occurs during infection with *L. monocytogenes*, was shown to promote general nuclear transport through phosphorylation of RanBP3 and, therefore, could be involved in SIRT2 relocalization (Yoon et al., 2008). Although the machinery for SIRT2 nuclear import remains to be determined, we show that S25 dephosphorylation is the signal required for chromatin association of SIRT2. Importantly, our data indicate that only isoform 1 of SIRT2 is able to bind to chromatin, as isoform 2 lacks S25, strongly suggesting that different isoforms have different localizations and functions. We, therefore, propose a two-step mechanism for SIRT2 localization during infection in which bacterial presence first induces the accumulation of SIRT2 in the nucleus and then an association with chromatin.

Interestingly, in non-resting cells, SIRT2 nuclear localization has been observed. For instance, SIRT2 accumulates in the nucleus in a cell-cycle-dependent manner and upon exposure to ionizing radiation (Inoue et al., 2007; Vaquero et al., 2006). Importantly for human health, SIRT2 nuclear localization was found to correlate with different cancer prognoses. In tissue samples from patients with glioblastoma, SIRT2 is mainly nuclear, but in control cells, it is predominantly cytoplasmic. Moreover, the higher the percentage of nuclear SIRT2, the more severe the patient prognosis (Imaoka et al., 2012). Here, we have identified a PTM, serine 25 phosphorylation, which is necessary for SIRT2 targeting and binding to chromatin and for H3K18 deacetylation. Therefore, along with reports correlating hypoacetylation of H3K18 with poor cancer prognosis (Manuyakorn et al., 2010; Seligson et al., 2009), we hypothesize that S25 could be a critical residue during cellular transformation and cancer.

Infection has revealed a role for SIRT2 in transcriptional repression, which is the function of the yeast homolog protein Sir2. Sequence analysis revealed that SIRT2 is localized in the same phylogenetic branch as Sir2 and SIRT1. Sir2 is a bona fide transcriptional repressor in yeast by being recruited to chromatin and causing silencing at repeated DNA sequences at the telomeres and mating-type or rDNA loci. Silencing requires the deacetylation of histones H3 and H4, and Sir2 shows high deacetylase activity toward these proteins (Blander and Guarente, 2004; North and Verdin, 2004). Interestingly, serine 25, along with surrounding serines 23 and 27 of SIRT2, is conserved in SIR2 of the fission yeast *Schizosaccharomyces pombe,* suggesting that phosphorylation might also regulate SIR2 function. To date, SIRT1 was considered to be the nuclear sirtuin and has been shown to associate with chromatin and work as a transcriptional repressor through its deacetylase activity (Jing and Lin, 2015). SIRT1 forms a repressive complex with a variety of chromatin-associated factors, such as the demethylase LSD1 (Mulligan et al., 2011). However, our studies with infection revealed that SIRT2, similarly to SIRT1 and yeast SIR2, functions in the nucleus as a transcriptional repressor.

PPM1A and PPM1B are metal-ion-binding phosphatases that belong to the PPM (protein phosphatase Mn2+/Mg2+) family and function as monomeric units (Lammers and Lavi, 2007). The observations that we report in this paper raise several questions. Indeed, by co-immunoprecipitation, we observe a complex forming between PPM1A, PPM1B, and SIRT2. In addition, our siRNA experiments show that knocking down either PPM1A or PPM1B abolishes the deacetylation of K18 observed upon infection. Taken together, these data suggest that the entire complex is necessary for SIRT2 function at the chromatin fraction, and loss of any one component disassembles the complex and blocks SIRT2 activity. In addition, as PPM1A is present in the nucleus in resting cells, we hypothesize that the complex forms in the nuclear compartment. The exact molecular mechanism of how this complex forms and whether it is necessary for other PPM1A/B substrates will have to be addressed. Another question that arises is in regard to how these phosphatases acquire specificity toward their substrate. Indeed, *Listeria* infection activates PPM1A and PPM1B to specifically target serine 25 and not serine 368 of SIRT2. Furthermore, another target of PPM1A, P65 (Lu et al., 2014), is not dephosphorylated during infection (Figure S6). How specificity is achieved remains to be determined but has been observed in many other systems (Lammers and Lavi, 2007). Our study adds SIRT2 to the list of substrates of PPM1A and PPM1B.

Our data reveal that infection relocalizes PPM1A and PPM1B, along with SIRT2, to chromatin during infection. In resting cells, the subcellular localization for PPM1A has been shown to be nuclear, while it is cytoplasmic for PPM1B (Chen et al., 2015; Li et al., 2015; Lin et al., 2006; Lu et al., 2014). Although PPM1B interacts with nuclear proteins and has a role in transcriptional regulation, PPM1B has only been found to localize to the nucleus during differentiation of adipocytes (Abraham et al., 2015; Prajapati et al., 2004; Tasdelen et al., 2013; Yien and Bieker, 2012). To our knowledge, infection with *L. monocytogenes* is the first exogenous stimulus that induces nuclear localization of PPM1B. Translocation and further co-immunoprecipitation of PPM1A and PPM1B with SIRT2 suggest that a complex between these proteins is formed during infection. Whether the complex forms in the cytoplasm with SIRT2 and PPM1B or once translocation to the nucleus has taken place remains to be determined.

In summary, among the new 21 PTMs of SIRT2 that we identified, we focused on S25 dephosphorylation, which is induced by *L. monocytogenes* infection in order to hijack SIRT2 and impose its role as a transcriptional modulator. We show that S25 is dephosphorylated during infection, but other stimuli could induce the same modification, thereby regulating the activity, substrate specificity, and subcellular localization of SIRT2. The relatively high number of PTMs identified for SIRT2 reflects the various functions of this protein in important cellular processes such as metabolism, aging, cancer, and senescence, and they deserve closer attention, as they could be the key to specific treatments for these diseases.

EXPERIMENTAL PROCEDURES

Antibodies

Antibodies used in this study are listed as follows; rabbit: anti-acetyl-histone H3K18 (Cell Signaling Technology, 9675), anti-histone H3 (Cell Signaling Technology, 9715), anti-GFP tag (Thermo Fisher Scientific, A-11122), anti-PPM1B (Abcam, ab137811), anti-PPM1B (Bethyl Laboratories, A300-887A), anti-Phospho-NF-κB p65 (Ser536) (93H1) (Cell Signaling Technology, #3033), anti-PP1 alpha (Upstate Biotechnology, #07-273), anti-CRM1 (H-300) (Santa Cruz Biotechnology, sc-5595), anti-SIRT2 (Abcam, ab67299), and anti-EF-Tu (Archambaud et al., 2005); mouse: anti-α-tubulin (Sigma, T6074), anti-PPM1A [p6c7] (Abcam, ab14824), anti-NFκB p65 (F-6) (Santa Cruz Biotechnology, sc-8008), and anti-FLAG M2 (F3165, Sigma).

Cell Culture, Infections, and Inhibitors

The bacterial strains that we used in this study are indicated in the Supplemental Experimental Procedures. *L. monocytogenes* strains were grown in brain-heart infusion medium (Difco Laboratories, Detroit, MI, USA) at 37°C. For infection experiments, bacteria were grown to mid-exponential phase, at an optical density 600 nm of 1.

HeLa (ATCC, CCL-2) cells were cultured in minimum essential medium (MEM) plus GlutaMAX (GIBCO, Waltham, MA, USA) supplemented with 1 mM sodium pyruvate (GIBCO), 0.1 mM nonessential amino acid solution (GIBCO), and 10% fetal bovine serum (FBS). MEFs were cultured in DMEM with 2 mM GlutaMAX (GIBCO) supplemented with 10% FBS. *Sirt2*$^{+/+}$ *and* *Sirt2*$^{-/-}$ primary MEFs were isolated from isogenic mice and transformed with a plasmid expressing SV40 large T antigen (BUG 3790).

For the purpose of infection experiments, HeLa cells and MEFs were grown to semiconfluence, at which point they were serum-starved for 24 hr and 30 min, respectively, before use. Exponential-phase bacteria were washed twice in PBS and added to cells at an MOI of 50:1, unless otherwise mentioned. After 1 hr of infection, cells were washed with serum-low medium, and 10 μg/mL gentamycin was added to kill extracellular bacteria. Infections were carried out for 5 hr and 24 hr.

For experiments involving pharmacological inhibitors, cells were pretreated for 24 hr prior to infection with DMSO or sanguinarine chloride (0.5 μM, Tocris, 2302).

Cloning

SIRT2-GFP, SIRT2-S25E-GFP (adjacent serine residues Ser23 → Glu23 and Ser27 → Glu27 were also mutated), SIRT2-S25A, and SIRT2-S368E-GFP were generated by PCR amplification of a G-block gene fragment (Integrated DNA Technologies) containing the sequence of WT SIRT2 isoform 1 cDNA (389 aa) using primers SIRT2 forward (fwd) and SIRT2 reverse (rev) and cloned at the EcoRI site of the pEGFP-N2 plasmid (Supplemental Experimental Procedures). SIRT2 isoform 2 (352 aa) was PCR-amplified with primers SIRT2-Iso2 fwd and SIRT2-rev from a GST-SIRT2 fusion (pGEX-4T2 backbone), which was a gift from Bernhard Lüscher: the resulting insert was cloned at the EcoRI site of the pEGFP-C1 vector. PPM1A-FLAG and PPM1B-FLAG were generated using G-blocks containing cDNA sequence, PCR-amplified, respectively, with primer pairs PPM1A-fw1/PPM1A-FLAG-rev and PPM1B-fw/PPM1B-FLAG-Rev (Supplemental Experimental Procedures), and cloned into the BamHI and NotI sites of the pCDNA 3.1(+) vector. Catalytically dead PPM1B [Arg^{179} → Gly^{179} (R179G)] was constructed by sewing reaction using the following primers: (1) PPM1B fwd/PPM1B 05 rev, (2) PPM1B 05/PPM1B-FLAG-rev, and (3) PPM1B fwd/PPM1B-FLAG-rev (Supplemental Experimental Procedures), followed by insertion at the EcoRI and NotI sites of the pcDNA3.1(+) vector. PPM1B-mRuby was generated by cloning PPM1B into the EcoRI site of the pmRuby2-C1 vector.

Transfections

HeLa cells were reverse transfected with commercial siRNA from Dharmacon (Lafayette, CO, USA) for PPM1A (ON-TARGETplus SMARTpool L-009574-00-0005) and PPM1B (ON-TARGETplus SMARTpool L-008281-01-0005), Pan PP1 (sc-43545, Santa Cruz Biotechnology), or control scramble siRNA (ON-TARGETplus Non-targeting Pool D-001810-10-05). Briefly, 25 nM siRNA is mixed with 4 μL Lipofectamine RNAiMAX (Invitrogen) in a 400-μL volume. After 15 min of incubation, 2×10^5 cells were added per well of a 6-well plate. Cells were assayed 48 and 72 hr after siRNA transfection.

For transfection of plasmid DNA, HeLa cells were seeded at a density of 2×10^5 cells per well of a 6-well plate the day prior to transfection. Briefly, 1.5 μg DNA (per well) was diluted in MEM without FBS and incubated with Lipofectamine LTX (Invitrogen) for 30 min. Lipofectamine-DNA complexes were incubated with cells for 4 hr and were assayed 48 hr after transfection. For larger scale transfection, volumes were adjusted proportionally.

MEFs were transfected using the Amaxa Mouse/Rat Hepatocyte Nucleofector Kit (Lonza, VPL-1004) or the jetPRIME Transfection Kit (Polyplus-transfection). Briefly, 1.5×10^6 cells (per well of a 6-well plate) were resuspended in 100 μL nucleofection solution and electroporated using an Amaxa Nucleofection II device (program T-30). jetPRIME transfections were performed according to the manufacturer's protocol. Cells were assayed 24 hr after transfection.

Immunoblotting and Cell Fractionation

Total cell lysates were harvested in 2× Laemmli buffer (124 mM Tris-Cl [pH 6.8], 4% SDS, 20% glycerol, 0.02% bromophenol blue, 0.03% DTT). Samples were boiled at 95°C for 5 min and sonicated for 5 s. After running on acrylamide gels, proteins were transferred using an iBLOT transfer system (Invitrogen) (program P0, 7 min), blocked in milk for 1 hr at room temperature and incubated with primary antibody overnight at 4°C. Membranes were washed in Tris-buffered saline-Tween (50 mM Tris [pH 8], 15 mM NaCl, 0.1% Tween) and incubated with horseradish-peroxidase-conjugated secondary antibody for 1 hr at room temperature, and blots were revealed with ECL-2 (Pierce, Waltham, MA, USA). Quantification of western blots was performed using the ChemiDoc (Bio-Rad) and associated software.

Cell fractionation was conducted as previously described (Eskandarian et al., 2013).

Immunofluorescence and Live-Cell Imaging

Cells were fixed in 4% paraformaldehyde (Electron Microscopy Sciences, Hatfield, PA, USA) for 10 min at room temperature and permeabilized in 0.3% Triton X-100 (Sigma) for 15 min. Coverslips were incubated with primary and secondary antibodies in 1% BSA + 0.1% Tween 100 and mounted on microscopy glass slides using Fluoromount G (Interchim, Montluçon, France). Images were acquired using an inverted wide-field fluorescence microscope (AxioVert 200M, Carl Zeiss Microscopy, Jena, Germany) equipped with an EMCCD Neo camera (Andor, Belfast, Northern Ireland) and the software MetaMorph (Molecular Devices, Sunnyvale, CA, USA). Live-cell imaging was performed for 120 min on a Zeiss Axio Observer spinning-disk confocal microscope equipped with a 63× oil objective and driven by the MetaMorph software. Images were acquired every 2 min for 2 hr.

qRT-PCR

Total mRNA was extracted using the RNeasy Kit (QIAGEN) and quantified using BioAnalyzer (Agilent). Reverse transcription (RT) was performed on 1 μg RNA with the iScript cDNA Synthesis Kit (Bio-Rad). qPCR was done on a 1:10 dilution of RT product using the SsoFast EvaGreen Supermix (Bio-Rad) and run on a MyIQ device (Bio-Rad). Data were analyzed using the Bio-Rad software and the ΔΔCt method.

Immunoprecipitation

Cells were scraped and lysed in RIPA buffer (10 mM Tris-Cl [pH 7.5], 150 mM NaCl, 0.5 mM EDTA, 0.1% SDS, 1% Triton X-100, 1% deoxycholate) supplemented with 25 U benzonase nuclease (Millipore), 1× cOmplete EDTA-free Protease Inhibitor Cocktail (Roche), and 1× PhosSTOP phosphatase inhibitor (Roche). Immunoprecipitations were performed overnight on a rotating wheel at 4°C. SIRT2-GFP was immunoprecipitated with GFP-TRAP agarose beads (ChromoTek), according to the manufacturer's protocol. Elution was performed by boiling the samples in Laemmli buffer + DTT. Immunoprecipitation of FLAG-tagged proteins was performed with Anti-FLAG M2 Magnetic Beads (Sigma), according to the manufacturer's protocol. FLAG-tagged proteins were eluted by competition with 100 μg/mL FLAG Peptide (F4799, Sigma). Drp1-FLAG construct (unpublished data) was used as a control.

Mass Spectometry Sample Preparation

Immunoprecipitated SIRT2-GFP from fractionated cells or whole-cell lysates was separated by SDS-PAGE on a 4%–15% polyacrylamide gel (Bio-Rad) and stained by colloid Coomassie blue (Invitrogen). From each sample, the SIRT2 gel band was excised and washed with H_2O, incubated for 15 min with water/acetonitrile (1:1, v/v), and incubated for 15 min with 100% acetonitrile before the band was dried completely in a vacuum concentrator. 0.25 μg sequencing-grade trypsin (Promega) in 50 mM ammonium bicarbonate in water/acetonitrile (9:1, v/v) was added to the dried gel slices, and proteins were digested overnight at 37°C. Peptides eluted from every gel slice were dried completely in a vacuum concentrator and re-dissolved in 20 μL solvent A (0.1% formic acid in water/acetonitrile; 98:2, v/v) for liquid chromatography-tandem MS (LC-MS/MS) analysis.

PTM Discovery by HCD Fragmentation

For accurate mapping of SIRT2 phosphorylation sites, samples were analyzed by LC-MS/MS on a Q Exactive instrument (Thermo Fisher Scientific) coupled to an EASY-nLC 1000 system (Thermo Fisher Scientific). 8 μL peptides in solvent A were loaded on a reverse-phase column (made in house, 75 μm inner diameter [i.d.] × 150 mm, 1.9-μm beads, ReproSil-Pur C18, Dr. Maisch, Ammerbuch-Entringen, Germany) and eluted by an increase in solvent B (0.1% formic acid in acetonitrile) in linear gradients from 2% to 30% in 55 min and then from 30% to 50% in 10 min, all at a constant flow rate of 300 nL/min. The mass spectrometer was operated in data-dependent mode, automatically switching between MS and MS/MS acquisition for the 10 most abundant ion peaks per MS spectrum. Full-scan MS spectra (300–2000 m/z) were acquired at a resolution of 70,000 after accumulation to a target value of 1,000,000, with a maximum fill time of 250 ms. The 10 most intense ions

above a threshold value of 10,000 were isolated (window of 2.0 Thompson [Th]) for HCD fragmentation at a normalized collision energy of 28% after filling the trap at a target value of 100,000 for a maximum of 100 ms with an underfill ratio of 1%. The S-lens RF level was set at 55, and we excluded precursor ions with single and unassigned charge states from fragmentation selection.

Data analysis was performed with MaxQuant (v1.5.6.5) (Cox and Mann, 2008) using the Andromeda search engine, with default search settings including a false discovery rate set at 1% on both the peptide and protein levels. Spectra were searched against the human proteins in the UniProtKB/Swiss-Prot database (database release version of January 2017 containing 20,172 human protein sequences; http://www.uniprot.org). The mass tolerances for precursor and fragment ions were set to 4.5 and 20 ppm, respectively, during the main search. Enzyme specificity was set as C-terminal to arginine and lysine, also allowing cleavage at proline bonds with a maximum of two missed cleavages. Variable modifications were set to oxidation of methionine residues; acetylation of protein N termini; acetylation of lysine residues; di-glycine modification of lysine residues; and phosphorylation of serine, threonine, and tyrosine residues. The minimum score for modified peptides was set to 20, and a minimum of 1 unique or razor peptide was required for protein identification. The SIRT2 modification sites in the GlyGly (K) sites, Phospho (STY) sites, and Acetyl (K) sites in MaxQuant are listed in Figure 1C.

Phosphosite Determination by ETD Fragmentation

For accurate mapping of the SIRT2 phosphorylation sites, samples were analyzed on an ETD-enabled LTQ Orbitrap Velos instrument (Thermo Fisher Scientific) coupled to an UltiMate 3000 RSLCnano UHPLC System (Thermo Fisher Scientific). 5 μL peptides in solvent A was loaded onto a C18 trap column (Acclaim PepMap 300, 5 μm, 300 Å, 300 μm i.d. × 5 mm; Thermo Fisher Scientific), desalted during 5 min, and then separated on a 20-cm homemade C18 column (3-μm particles, Dr. Maisch, Ammerbuch-Entringen, Germany) by a one-step gradient (from 2.0% to 65% solvent B (0.1% formic acid in water/acetonitrile [20:80, v/v]) in 59 min, all at a constant flow rate of 300 nL/min. MS data were acquired using Xcalibur software (v2.1) with a survey scan (300–2,000 m/z) analyzed into the Orbitrap mass analyzer at a resolution setting of 60,000 in profile mode. ETD fragmentation was triggered for the 15 most intense precursor ions included in a parent mass list corresponding to the different forms of S368 and S25 peptides. Fragments were analyzed in the linear ion trap. The automatic gain control (AGC) targets for MS and MS/MS scans were set to 1,000,000 and 5,000, respectively. The isolation width was set to 2.0 m/z, and the activation time was set to 150 ms. Selected ions were dynamically excluded for 15 s.

The ion chromatograms of the peptides of interest (XICs) were extracted manually using the Qual Browser software in Xcalibur (v2.2). Extracted ion current was searched at 5 ppm in MS1, and all XIC values were normalized over the full total ion current of the injection. For peptide annotation, raw data files were analyzed using the MaxQuant software, v.1.5.3.8 (Cox and Mann, 2008), with the Andromeda search engine (Cox et al., 2011). The acquisitions were searched against a human database (UniProt databases containing 89,706 entries, including 42,034 SwissProt entries, downloaded on January 13, 2015). The digestion mode was set to trypsin, and a maximum of two missed cleavages were allowed. N-terminal acetylation and methionine oxidation were set as variable modifications, and cysteine carbamidomethylation was set as fixed modification. For the phosphorylation of S25- and S368-containing peptides, additional phosphorylation of S/T/Y was set to variable modification. False discovery rates were fixed at 1% at both peptide and protein levels.

Statistical Analysis

The p values were calculated using a paired Student's t test. Values of $p < 0.05$ were considered significant. Values of $p < 0.05$ were ranked as $^{*}p < 0.05$, $^{**}p < 0.01$, and $^{***}p < 0.001$.

SUPPLEMENTAL INFORMATION

Supplemental Information includes Supplemental Experimental Procedures and seven figures and can be found with this article online at https://doi.org/10.1016/j.celrep.2018.03.116.

ACKNOWLEDGMENTS

We thank B. Lüscher for providing the SIRT2 isoform 2 plasmid. Work in the M.A.H. laboratory received financial support from Institut Pasteur and the National Research Agency (ANR-EPIBACTIN). Work in the P.C. laboratory received financial support from Institut Pasteur, INSERM, INRA, the National Research Agency (ANR; ERANET Infect-ERA PROANTILIS ANR-13-IFEC-0004-02), the French Government's Investissement d'Avenir program, the Laboratoire d'Excellence "Integrative Biology of Emerging Infectious Diseases" (ANR-10-LABX-62-IBEID), the European Research Council (ERC; H2020-ERC-2014-ADG 670823-BacCellEpi), the Fondation le Roch les Mousquetaires, and the Fondation Balzan. P.C. is a Senior International Research Scholar of the Howard Hughes Medical Institute. The authors have no other relevant affiliations or financial involvement with any organization or entity with a financial interest in or financial conflict with the subject matter or materials discussed in the manuscript apart from those disclosed.

AUTHOR CONTRIBUTIONS

Conceptualization, J.M.P., M.A.H., P.C., T.C., F.I., and M.M.; Methodology, J.M.P., T.C., and F.I.; Software, Q.G.; Formal Analysis, J.M.P., C.C., and Q.G.; Investigation, J.M.P., T.C., and F.I.; Resources, P.C.; Writing – Original Draft, J.M.P. and M.A.H.; Writing – Review & Editing, J.M.P., M.A.H., P.C., T.C., and F.I.; Supervision, M.A.H. and P.C.

DECLARATION OF INTERESTS

The authors declare no competing interests.

Received: September 13, 2017
Revised: February 1, 2018
Accepted: March 26, 2018
Published: April 24, 2018

REFERENCES

Abraham, S., Paknikar, R., Bhumbra, S., Luan, D., Garg, R., Dressler, G.R., and Patel, S.R. (2015). The Groucho-associated phosphatase PPM1B displaces Pax transactivation domain interacting protein (PTIP) to switch the transcription factor Pax2 from a transcriptional activator to a repressor. J. Biol. Chem. *290*, 7185–7194.

Aburai, N., Yoshida, M., Ohnishi, M., and Kimura, K. (2010). Sanguinarine as a potent and specific inhibitor of protein phosphatase 2C in vitro and induces apoptosis via phosphorylation of p38 in HL60 cells. Biosci. Biotechnol. Biochem. *74*, 548–552.

Archambaud, C., Gouin, E., Pizarro-Cerda, J., Cossart, P., and Dussurget, O. (2005). Translation elongation factor EF-Tu is a target for Stp, a serine-threonine phosphatase involved in virulence of Listeria monocytogenes. Mol. Microbiol. *56*, 383–396.

Blander, G., and Guarente, L. (2004). The Sir2 family of protein deacetylases. Annu. Rev. Biochem. *73*, 417–435.

Cha, Y., Han, M.-J., Cha, H.-J., Zoldan, J., Burkart, A., Jung, J.H., Jang, Y., Kim, C.-H., Jeong, H.-C., Kim, B.-G., et al. (2017). Metabolic control of primed human pluripotent stem cell fate and function by the miR-200c-SIRT2 axis. Nat. Cell Biol. *19*, 445–456.

Chen, W., Wu, J., Li, L., Zhang, Z., Ren, J., Liang, Y., Chen, F., Yang, C., Zhou, Z., Su, S.S., et al. (2015). Ppm1b negatively regulates necroptosis through dephosphorylating Rip3. Nat. Cell Biol. *17*, 434–444.

Chi, A., Huttenhower, C., Geer, L.Y., Coon, J.J., Syka, J.E.P., Bai, D.L., Shabanowitz, J., Burke, D.J., Troyanskaya, O.G., and Hunt, D.F. (2007). Analysis of phosphorylation sites on proteins from *Saccharomyces cerevisiae* by electron transfer dissociation (ETD) mass spectrometry. Proc. Natl. Acad. Sci. USA *104*, 2193–2198.

Cossart, P. (2011). Illuminating the landscape of host-pathogen interactions with the bacterium Listeria monocytogenes. Proc. Natl. Acad. Sci. USA *108*, 19484–19491.

Cox, J., and Mann, M. (2008). MaxQuant enables high peptide identification rates, individualized p.p.b.-range mass accuracies and proteome-wide protein quantification. Nat. Biotechnol. *26*, 1367–1372.

Cox, J., Neuhauser, N., Michalski, A., Scheltema, R.A., Olsen, J.V., and Mann, M. (2011). Andromeda: a peptide search engine integrated into the MaxQuant environment. J. Proteome Res. *10*, 1794–1805.

de Oliveira, R.M., Sarkander, J., Kazantsev, A.G., and Outeiro, T.F. (2012). SIRT2 as a therapeutic target for age-related disorders. Front. Pharmacol. *3*, 82.

Eskandarian, H.A., Impens, F., Nahori, M.-A., Soubigou, G., Coppée, J.-Y., Cossart, P., and Hamon, M.A. (2013). A role for SIRT2-dependent histone H3K18 deacetylation in bacterial infection. Science *341*, 1238858.

Flick, F., and Lüscher, B. (2012). Regulation of sirtuin function by posttranslational modifications. Front. Pharmacol. *3*, 29.

Gomes, P., Fleming Outeiro, T., and Cavadas, C. (2015). Emerging role of sirtuin 2 in the regulation of mammalian metabolism. Trends Pharmacol. Sci. *36*, 756–768.

Hornbeck, P.V., Zhang, B., Murray, B., Kornhauser, J.M., Latham, V., and Skrzypek, E. (2015). PhosphoSitePlus, 2014: mutations, PTMs and recalibrations. Nucleic Acids Res. *43*, D512–D520.

Imaoka, N., Hiratsuka, M., Osaki, M., Kamitani, H., Kambe, A., Fukuoka, J., Kurimoto, M., Nagai, S., Okada, F., Watanabe, T., et al. (2012). Prognostic significance of sirtuin 2 protein nuclear localization in glioma: an immunohistochemical study. Oncol. Rep. *28*, 923–930.

Inoue, T., Hiratsuka, M., Osaki, M., Yamada, H., Kishimoto, I., Yamaguchi, S., Nakano, S., Katoh, M., Ito, H., and Oshimura, M. (2007). SIRT2, a tubulin deacetylase, acts to block the entry to chromosome condensation in response to mitotic stress. Oncogene *26*, 945–957.

Jing, H., and Lin, H. (2015). Sirtuins in epigenetic regulation. Chem. Rev. *115*, 2350–2375.

Kusuda, K., Kobayashi, T., Ikeda, S., Ohnishi, M., Chida, N., Yanagawa, Y., Shineha, R., Nishihira, T., Satomi, S., Hiraga, A., and Tamura, S. (1998). Mutational analysis of the domain structure of mouse protein phosphatase 2Cbeta. Biochem. J. *332*, 243–250.

Lammers, T., and Lavi, S. (2007). Role of type 2C protein phosphatases in growth regulation and in cellular stress signaling. Crit. Rev. Biochem. Mol. Biol. *42*, 437–461.

Li, Z., Liu, G., Sun, L., Teng, Y., Guo, X., Jia, J., Sha, J., Yang, X., Chen, D., and Sun, Q. (2015). PPM1A regulates antiviral signaling by antagonizing TBK1-mediated STING phosphorylation and aggregation. PLoS Pathog. *11*, e1004783.

Lin, X., Duan, X., Liang, Y.Y., Su, Y., Wrighton, K.H., Long, J., Hu, M., Davis, C.M., Wang, J., Brunicardi, F.C., et al. (2006). PPM1A functions as a Smad phosphatase to terminate TGFbeta signaling. Cell *125*, 915–928.

Lu, X., An, H., Jin, R., Zou, M., Guo, Y., Su, P.-F., Liu, D., Shyr, Y., and Yarbrough, W.G. (2014). PPM1A is a RelA phosphatase with tumor suppressor-like activity. Oncogene *33*, 2918–2927.

Manuyakorn, A., Paulus, R., Farrell, J., Dawson, N.A., Tze, S., Cheung-Lau, G., Hines, O.J., Reber, H., Seligson, D.B., Horvath, S., et al. (2010). Cellular histone modification patterns predict prognosis and treatment response in resectable pancreatic adenocarcinoma: results from RTOG 9704. J. Clin. Oncol. *28*, 1358–1365.

Martin, M., Kettmann, R., and Dequiedt, F. (2007). Class IIa histone deacetylases: regulating the regulators. Oncogene *26*, 5450–5467.

Michan, S., and Sinclair, D. (2007). Sirtuins in mammals: insights into their biological function. Biochem. J. *404*, 1–13.

Mulligan, P., Yang, F., Di Stefano, L., Ji, J.Y., Ouyang, J., Nishikawa, J.L., Toiber, D., Kulkarni, M., Wang, Q., Najafi-Shoushtari, S.H., et al. (2011). A SIRT1-LSD1 corepressor complex regulates Notch target gene expression and development. Mol. Cell *42*, 689–699.

Nahhas, F., Dryden, S.C., Abrams, J., and Tainsky, M.A. (2007). Mutations in SIRT2 deacetylase which regulate enzymatic activity but not its interaction with HDAC6 and tubulin. Mol. Cell. Biochem. *303*, 221–230.

North, B.J., and Verdin, E. (2004). Sirtuins : Sir2-related NAD-dependent protein deacetylases. Genome Biol. *5*, 224.

North, B.J., and Verdin, E. (2007a). Interphase nucleo-cytoplasmic shuttling and localization of SIRT2 during mitosis. PLoS ONE *2*, e784.

North, B.J., and Verdin, E. (2007b). Mitotic regulation of SIRT2 by cyclin-dependent kinase 1-dependent phosphorylation. J. Biol. Chem. *282*, 19546–19555.

North, B.J., Marshall, B.L., Borra, M.T., Denu, J.M., and Verdin, E. (2003). The human Sir2 ortholog, SIRT2, is an NAD+-dependent tubulin deacetylase. Mol. Cell *11*, 437–444.

Prajapati, S., Verma, U., Yamamoto, Y., Kwak, Y.T., and Gaynor, R.B. (2004). Protein phosphatase 2Cbeta association with the IkappaB kinase complex is involved in regulating NF-kappaB activity. J. Biol. Chem. *279*, 1739–1746.

Rothgiesser, K.M., Erener, S., Waibel, S., Lüscher, B., and Hottiger, M.O. (2010). SIRT2 regulates NF-κB dependent gene expression through deacetylation of p65 Lys310. J. Cell Sci. *123*, 4251–4258.

Schaaf, K., Smith, S.R., Duverger, A., Wagner, F., Wolschendorf, F., Westfall, A.O., Kutsch, O., and Sun, J. (2017). *Mycobacterium tuberculosis* exploits the PPM1A signaling pathway to block host macrophage apoptosis. Sci. Rep. *7*, 42101.

Seligson, D.B., Horvath, S., McBrian, M.A., Mah, V., Yu, H., Tze, S., Wang, Q., Chia, D., Goodglick, L., and Kurdistani, S.K. (2009). Global levels of histone modifications predict prognosis in different cancers. Am. J. Pathol. *174*, 1619–1628.

Tasdelen, I., van Beekum, O., Gorbenko, O., Fleskens, V., van den Broek, N.J.F., Koppen, A., Hamers, N., Berger, R., Coffer, P.J., Brenkman, A.B., and Kalkhoven, E. (2013). The serine/threonine phosphatase PPM1B (PP2Cβ) selectively modulates PPARγ activity. Biochem. J. *451*, 45–53.

Terry, L.J., Shows, E.B., and Wente, S.R. (2007). Crossing the nuclear envelope: hierarchical regulation of nucleocytoplasmic transport. Science *318*, 1412–1416.

Vaquero, A., Scher, M.B., Lee, D.H., Sutton, A., Cheng, H.L., Alt, F.W., Serrano, L., Sternglanz, R., and Reinberg, D. (2006). SirT2 is a histone deacetylase with preference for histone H4 Lys 16 during mitosis. Genes Dev. *20*, 1256–1261.

Xu, L., and Massagué, J. (2004). Nucleocytoplasmic shuttling of signal transducers. Nat. Rev. Mol. Cell Biol. *5*, 209–219.

Yien, Y.Y., and Bieker, J.J. (2012). Functional interactions between erythroid Krüppel-like factor (EKLF/KLF1) and protein phosphatase PPM1B/PP2Cβ. J. Biol. Chem. *287*, 15193–15204.

Yoon, S.O., Shin, S., Liu, Y., Ballif, B.A., Woo, M.S., Gygi, S.P., and Blenis, J. (2008). Ran-binding protein 3 phosphorylation links the Ras and PI3-kinase pathways to nucleocytoplasmic transport. Mol. Cell *29*, 362–375.